Slow-Binding Inhibition of the Aminopeptidase from *Aeromonas proteolytica* by Peptide Thiols: Synthesis and Spectroscopic Characterization†

Kristi M. Huntington,‡,§ David L. Bienvenue,‡,|| Yaoming Wei,‡,§ Brian Bennett,‡,||,⊥ Richard C. Holz,*,|| and Dehua Pei*,§

Department of Chemistry and Ohio State Biochemistry Program, The Ohio State University, 100 West 18th Avenue, Columbus, Ohio 43210, and Department of Chemistry and Biochemistry, Utah State University, Logan, Utah 84322

Received June 4, 1999; Revised Manuscript Received September 23, 1999

ABSTRACT: Peptide-derived thiols of the general structure *N*-mercaptoacyl-leucyl-*p*-nitroanilide (**1a**−**c**) were synthesized and found to be potent, slow-binding inhibitors of the aminopeptidase from *Aeromonas proteolytica* (AAP). The overall potencies (K_I*) of these inhibitors against AAP range from 2.5 to 57 nM exceeding that of the natural product bestatin and approaching that of amastatin. The corresponding alcohols (**2a**−**b**) are simple competitive inhibitors of much lower potencies (K_I = 23 and 360 μM). These data suggest that the free thiols are involved in the formation of the E·I and E·I* complexes, presumably serving as a metal ligand. To investigate the nature of the interaction of the thiol-based inhibitors with the dinuclear active site of AAP, we have recorded electronic absorption and EPR spectra of Co(II)Co(II)-, Co(II)Zn(II)-, and Zn(II)Co(II)-AAP in the presence of the strongest binding inhibitor, **1c**. Both [CoZn-(AAP)] and [ZnCo(AAP)], in the presence of **1c**, exhibited an absorption band centered at 320 nm characteristic of an S → Co(II) ligand−metal charge-transfer band. In addition, absorption spectra recorded between 400 and 700 nm showed changes characteristic of **1c** interacting with each active-site metal ion. EPR spectra recorded at high temperature (19 K) and low power (2.5 mW) indicated that in a given enzyme molecule, **1c** interacts weakly with one of the metal ions in the dinuclear site and that the crystallographically identified μ-OH(H) bridge, which has been shown to mediate electronic interaction of the Co(II) ions, is likely broken upon **1c** binding. EPR spectra of [CoCo(AAP)]-**1c**, [ZnCo(AAP)]-**1c**, and [CoZn(AAP)]-**1c** were also recorded at lower temperature (3.5−4.0 K) and high microwave power (50−553 mW). The observed signals were unusual and appeared to contain, in addition to the incompletely saturated contributions from the signals characterized at 19 K, a very sharp feature at $g_{eff} \approx 6.8$ that is characteristic of thiolate-Co(II) interactions. These data suggest that the thiolate moiety can bind to either of the metal ions in the dinuclear active site of AAP but does not bridge the dinuclear cluster. Compounds **1a**−**c** are readily accessible by synthesis and thus provide a novel class of potent aminopeptidase inhibitors.

Aminopeptidases are a group of exopeptidases that catalyze the hydrolysis of a wide range of N-terminal amino acid residues from proteins and polypeptides (*1*−*3*). These enzymes are widely distributed in bacteria, yeast, plant, and animal tissues and, therefore, have a wide variety of biological functions such as protein maturation, protein degradation, hormone level regulation, and cell-cycle control (*3*). The importance of understanding the mechanism of action of aminopeptidases is underscored by the recent observation that the naturally occurring peptide analogue inhibitor, bestatin, was shown to significantly decrease HIV viral load in men by inhibiting leucine aminopeptidase activity (*4*). Abnormal aminopeptidase activity has also been associated with many health conditions and pathologies including aging, cataracts, inflammation, cystic fibrosis, cancer, and leukemia; thus, their biological and medicinal significance is immense (*1*−*3*). In addition, recent studies on the biochemical pathways involved in metastasis have revealed a set of proteinases and genes that play important roles in tumor growth and proliferation (*5*, *6*). Aminopeptidase activity has been reported on the surface of tumor cells (*7*), suggesting that aminopeptidases play essential roles in the metastatic process, particularly in the steps involving tumor cells traversing the basement membrane and collagenous stroma. A recent study has shown that several naturally occurring aminopeptidase inhibitors (i.e., bestatin, leuhistin, and actinonin) inhibit matrix degradation and invasion of extracellular matrixes by fibrosarcoma cells (*8*). Another role for aminopeptidases in tumor cell growth involves angiogenesis, the formation of new blood vessels, which is essential for tumor growth (*9*). Recently, the type-2 methionine aminopeptidase (MetAP) from eukaryotes has been identified as the molecular target for the anti-angiogenesis

† This work was supported by the National Institutes of Health (AI40575 to D.P.) and the National Science Foundation (CHE-9816487 to R.C.H.). The Bruker ESP-300E EPR spectrometer was purchased with funds provided by the National Science Foundation (BIR-9413530) and Utah State University.

* To whom correspondence should be addressed. (D.P.) Phone: (614) 688-4068. Fax: (614) 292-1532. E-mail: pei.3@osu.edu. (R.C.H.) Phone: (435) 797-2609. Fax: (435) 797-3390. E-mail: rholz@cc.usu.edu.

‡ These authors contributed equally to this work.

§ The Ohio State University.

|| Utah State University.

⊥ Present address: CCLRC Daresbury Laboratory, Warrington, WA4 4AD, U.K.

10.1021/bi991283e CCC: $18.00
Published on Web 10/30/1999

drugs ovalicin and fumagillin (*9*−*13*). Thus, the inhibition of aminopeptidase activity in viruses and at malignant tumors is critically important in preventing the growth and proliferation of these types of cells and, for this reason, have become the subject of intense efforts in inhibitor design.

The aminopeptidase from the marine bacterium *Aeromonas proteolytica* (AAP)[1] possesses ideal properties for studying hydrolytic reactions catalyzed by metallo-aminopeptidases (*14*). AAP is a small, monomeric enzyme (29 500 Da) that contains two Zn(II) ions per mole of polypeptide and is thermostable for several hours at 70 °C (*14*). It has been crystallographically characterized and contains a (μ-aqua)-(μ-carboxylato)dizinc(II) core with a single histidine and carboxylate residue at each metal site (*15*). Substitution of the two Zn(II) ions with Co(II), Cu(II), or Ni(II) provides enzymes that are hyperactive by 7.7, 6.5, and 25 times, respectively, toward certain substrates (*16*−*18*). Bennett and Holz (*19*) recently demonstrated that metal binding to apo-AAP occurs in a sequential fashion, highlighting the potential formation of heterodimetallic sites. Catalytically competent heterodimetallic centers provide systems in which the function of each metal ion can be independently studied by labeling the metal-binding sites with spectroscopically active and silent metal ions, respectively. Several inhibitors of AAP have been studied in this way, and these molecules can be classified into three types: substrate analogues, tetrahedral transition-state analogues, and simple metal-chelating agents. Examples of the former two types include boronic acids (*20*−*22*), chloromethyl ketones (*14*), and phosphonic acids (*23*−*25*). Among the metal chelators, hydroxamates (*26*−*28*) and α-hydroxyamides (*14*) have been shown to be particularly potent inhibitors of AAP. However, despite the wide-spread use of thiols in designing metalloenzyme inhibitors (*29*−*31*), the use of thiols as aminopeptidase inhibitors is rare (*32*−*34*). Here we report that peptide-derived thiols are potent, slow-binding inhibitors of AAP. Spectroscopic characterization of the AAP-inhibited complexes reveal that peptide thiols interact with each active-site metal ion.

MATERIALS AND METHODS

Materials. 4-Mercaptobutyric acid was purchased from Karl Industries Inc. (Aurora, OH). Hepes buffer, L-Leucyl *p*-nitroanalide (Leu-*p*NA), and cobalt chloride were purchased from Sigma. Zinc sulfate was from J. T. Baker. Tris-(2-carboxyethyl)phosphine hydrochloride (TCEP) was purchased from Boehringer Mannheim Laboratories. All other reagents used in this work were purchased from either Aldrich or Sigma.

Inhibitor Synthesis. All of the coupling reactions between acids and Leu-*p*NA were carried out with *O*-benzotriazol-1-yl-*N*,*N*,*N*′,*N*′-tetramethyluronium hexafluorophosphate (HBTU) except for 3-methoxypropionic acid, which was coupled to Leu-pNA with dicyclohexylcarbodiimide (DCC). Products were purified by silica gel or a combination of silica gel and alumina columns. The commercial 4-mercaptobutytic acid contained a large amount of thiolactone and the oxidized disulfide dimer. The commercial sample was treated with NaOH to open the thiolactone ring, and then triphenylphosphine was used to reduce the disulfide bond before use. Mercaptoacetic acid was oxidized to its dimer form with hydrogen peroxide prior to its use in the coupling reaction. 3-Methoxypropionylleucyl-*p*-nitroanilide was treated with BBr_3 at 0 °C to cleave the methyl ether bond (*35*).

N-(Glycolyl)leucyl-*p*-nitroanilide (**2a**): ^{1}H NMR (200 MHz, $CDCl_3$) δ 9.60 (s, 1H), 8.06 (d, J = 9.2 Hz, 2H), 7.59 (d, J = 9.2 Hz, 2H), 7.20 (d, J = 7.5 Hz, 1H), 4.62−4.73 (m, 1H), 4.21 (s, 2H), 3.18 (s, 1H), 1.55−1.95 (m, 3H), 0.80−1.10 (m, 6H). MS (FAB) *m*/*z* observed, 310 ($M + H^+$); calcd, 309.

N-(3-Hydroxylpropionyl)leucyl-*p*-nitroanilide (**2b**): ^{1}H NMR (200 MHz, $CDCl_3$) δ 9.59 (s, 1H), 8.06 (d, J = 9.2 Hz, 2H), 7.61 (d, J = 9.2 Hz, 2H), 6.82 (d, J = 7.6 Hz, 1H), 4.60−4.73 (m, 1H), 3.94 (t, J = 5.2 Hz, 2H), 3.08 (s, 1H), 2.47−2.60 (t, J = 5.5 Hz, 3H), 1.50−1.90 (m, 3H), 0.80−1.06 (m, 6H). MS (FAB) *m*/*z* observed, 324 ($M + H^+$); calcd, 323.

2,2′-Dithiobis(*N*-acetylleucyl-*p*-nitroanilide) (dimer of **1a**): ^{1}H NMR (200 MHz, DMSO) δ 10.73 (s, 1H), 8.44 (d, J = 7.5 Hz, 1H), 8.21 (d, J = 9.2 Hz, 2H), 7.84 (d, J = 9.2 Hz, 2H), 4.35−4.58 (m, 1H), 3.56 (d, J = 2.7 Hz, 2H), 1.40−1.80 (m, 3H), 0.80−0.99 (m, 6H). MS (FAB) *m*/*z* observed, 649 ($M + H^+$); calcd, 648.

N-(3-Mercaptopropionyl)leucyl-*p*-nitroanilide (**1b**): ^{1}H NMR (250 MHz, $CDCl_3$) δ 9.55 (s, 1H), 8.08 (d, J = 9.2 Hz, 2H), 7.61 (d, J = 9.2 Hz, 2H), 6.44 (d, J = 7.9 Hz, 1H), 4.60−4.79 (m, 1H), 2.72−2.95 (m, 2H), 2.50−2.72 (m, 2H), 1.54−1.93 (m, 4H), 0.80−1.12 (m, 6H). MS (FAB) *m*/*z* observed, 340 ($M + H^+$); calcd, 339.

N-(4-Mercaptobutyryl)leucyl-*p*-nitroanilide (**1c**): ^{1}H NMR (300 MHz, $CDCl_3$) δ 9.46 (s, 1H), 8.00−8.19 (m, 2H), 7.53−7.77 (m, 2H), 6.15 (d, J = 7.9 Hz, 1H), 4.52−4.75 (m, 1H), 2.25−2.72 (m, 4H), 1.98 (t, J = 8.2 Hz, 1H), 1.55−1.90 (m, 5H), 0.83−1.10 (m, 6H). MS (FAB) *m*/*z* observed, 354 ($M + H^+$); calcd, 353.

N-(4-Mercaptobutyryl)leucylanilide (**1d**): ^{1}H NMR (250 MHz, $CDCl_3$) δ 9.44 (s, 1H), 7.52 (d, J = 8.2 Hz, 2H), 7.22 (t, J = 7.9 Hz, 2H), 7.07 (t, J = 7.4 Hz, 1H), 4.81 (m, 1H), 3.50 (m, 1H), 2.62 (t, J = 7.1 Hz, 2H), 2.20−2.50 (m, 2H), 1.60−2.00 (m, 5H), 1.01 (d, J = 5.5 Hz, 3H), 0.97 (d, J = 5.5 Hz, 3H).

Purification of AAP. The aminopeptidase from *A. proteolytica* was purified from a stock culture kindly provided by Professor Céline Schalk (*36*). Cultures were grown according to the previously published procedure (*14*) with minor modifications to the growth media (*37*). Enzyme was purified as previously described (*19*). Purified enzyme was stored at −80 °C until needed.

Spectrophotometric Assay of AAP. AAP activity was measured by the method of Prescott and Wilkes (*14*) as modified by Baker et al. (*21*). In this assay, the hydrolysis of 0.5 mM Leu-*p*NA (in 50 mM Hepes, pH 7.5, 50 mM NaCl, 100 μM $ZnSO_4$, and 1 mM TCEP) was measured spectrophotometrically at 25 °C by monitoring the formation of *p*-nitroaniline. The extent of hydrolysis was calculated by monitoring the increase in absorbance at 405 nm ($\Delta\epsilon_{405}$ value of *p*-nitroaniline of 10 800 M^{-1} cm^{-1}) (*38*). One unit

[1] Abbreviations: AAP, aminopeptidase from *Aeromonas proteolytica*; blLAP, bovine lens leucine aminopeptidase; MAP, methionyl aminopeptidase from *E. coli*; AMPP, aminopeptidase-P from *E. coli*; Hepes, [4-(2-hydroxyethyl)-1-piperazineethanesulfonic acid]; Tricine, *N*-tris[hydroxymethyl]methylglycine; LMCT, ligand-to-metal charge-transfer; TCEP, tris(2-carboxyethyl)phosphine, hydrochorlide; Leu-*p*NA, L-leucyl-*p*-nitroanilide.

was defined as the amount of enzyme that releases 1 μmol of *p*-nitroaniline at 25 °C in 60 s. The specific activity of purified AAP was typically found to be 120 units/mg of enzyme. This value is identical to that reported by Prescott and Wilkes (*14*). Enzyme concentrations were determined from the absorbance at 278 nm with the value $\epsilon_{278} = 41\,800$ M^{-1} cm^{-1} (*39*). TCEP (final 1 mM) was added to all assay reactions in order to keep the peptide thiols in the reduced form; this concentration of TCEP had no effect on AAP activity or stability.

*Slow Binding Inhibition of AAP by Thiol Inhibitors **1a**−**d***. Inhibitors **1a**−**d** were freshly dissolved in 60:40 MeOH/water (v/v) to give 0.1−1 mM stock solutions. Their concentrations (**1a**−**c**) were determined by hydrolyzing the *p*-nitroanilide group to completion with 1 N NaOH and quantitating the released *p*-nitroaniline at 405 nm. Prior to use, 10 mM TCEP was added to the stock solution to reduce any disulfide which might have formed during storage (**1a** was synthesized as the disulfide linked dimer). Assays were carried out in 50 mM Hepes, pH 7.5, 50 mM NaCl, 100 μM $ZnSO_4$, 1 mM TCEP, and appropriate concentrations of the inhibitors (0−14 μM) with 500 μM leucyl-*p*-nitroanilide (Leu-*p*NA) as substrate. To determine the equilibrium constants K_I and K_I*, the reaction was initiated by the addition of AAP (83−140 ng/mL) to the above mixture and the release of *p*-nitroaniline was monitored at 405 nm in a Perkin-Elmer UV−vis spectrophotometer (none of the inhibitors act as substrate of AAP). The initial rate v_0 and the steady-state rate v_s were determined by fitting the data against eq 1

$$\text{Abs} = v_s t + (v_0 - v_s)(1 - e^{-kt})/k \quad (1)$$

where k is the observed first-order rate constant for the isomerization of the weak complex to the tight complex at a particular concentration (*40*). A secondary plot of v_0 vs [I] gave the dissociation constant K_I according to eq 2

$$v_0 = V \cdot [S]/(K_M(1 + [I]/K_I) + [S]) \quad (2)$$

where V is maximum velocity and K_M is the Michaelis constant (*40*). A similar plot of v_s vs [I] gave the dissociation constant K_I*.

To determine the dissociation rate constant k_6, AAP (320 nM) was preincubated for 1 h at 0 °C in the presence of **1a**−**d** (10 μM final concentration). This preincubated enzyme was then used to initiate the reaction by adding it to a reaction mixture containing 50 mM Hepes, pH 7.5, 50 mM NaCl, 100 μM $ZnSO_4$, 1 mM TCEP, and 500 μM Leu-*p*NA. The recovered AAP activity was monitored at 405 nm and the absorbance vs time data were fit to the eq 3:

$$\text{Abs} = v_s [t - (1 - e^{k_6 t})/k_6] \quad (3)$$

*Competitive Inhibition by Hydroxy Inhibitors **2a,b***. All assays were carried out in 50 mM Hepes, pH 7.5, 50 mM NaCl, and 100 μM $ZnSO_4$ using Leu-*p*NA as substrate (20−320 μM) in the presence of 0−400 μM inhibitor (total volume of 1.0 mL). The reaction was initiated by the addition of AAP (83−140 ng) to the reaction mixture and *p*-nitroaniline formation was monitored as before over 5 min. The initial rates were calculated from the early regions of the reaction progress curves and then plotted against substrate concentration, from which the apparent Michaelis constant, K_M', was determined. The inhibition constant K_i was obtained by plotting K_M' vs [I] and fitting the data against eq 4:

$$K_M' = K_M (1 + [I]/K_I) \quad (4)$$

Co(II)-Substituted AAP Samples. [CoCo(AAP)], [CoZn(AAP)], and [ZnCo(AAP)] were prepared from the purified enzyme by a method similar to that of Prescott et al. (*17*) and Bennett and Holz (*41*). AAP was dialyzed for 72 h at 4 °C against 10 mM 1,10-phenanthroline monohydrochloride in 50 mM Hepes buffer (pH 7.5) and then exhaustively dialyzed against chelex-treated Hepes buffer. Metal insertion was effected by direct addition, with efficient mixing, of 1 equiv of MCl_2 (where M = Co or Zn; ≥ 99.999% $CoCl_2$, Strem Chemicals, Newburyport, Massachusetts; 99.999% $ZnCl_2$, Aldrich) followed by a 30 min incubation period at 20−25 °C. The second metal was then inserted in the same manner, and the electronic absorption spectrum recorded. The inhibitor **1c** (20 μL of a 10 mM stock solution + TCEP) was introduced onto the side-wall of an anaerobic cuvette, and the enzyme sample introduced. As earlier work has demonstrated by optical methods (*42*), violently flicking the above system facilitates rapid and efficient mixing of the reagents.

Spectroscopic Measurements. All spectrophotometric measurements were performed on a Shimadzu UV-3101PC spectrophotometer equipped with a constant temperature holder and a Haake (Type 423) constant temperature circulating bath. The use of 200 μL, 1 cm path-length microcuvettes (QS, Hellma) sealed with a rubber septa, facilitated the recording of the optical spectra under anaerobic conditions. Subtraction of the absorption spectrum of apo-AAP from those of substituted enzyme samples, was performed using Shimadzu UV-3101 software. Enzyme concentrations for electronic absorption studies were typically 1 mM. Low-temperature dual mode EPR spectroscopy was carried out as in earlier work (*19*, *41*) using a Bruker ESP-300E spectrometer equipped with an ER 4116 DM dual mode X-band cavity and an Oxford Instruments ESR-900 helium flow cryostat. EPR spectra were recorded at a modulation frequency of 100 kHz with microwave frequencies of about 9.65 and 9.37 GHz for perpendicular and parallel mode, respectively. Precise microwave frequencies were recorded for individual spectra to ensure exact *g*-alignment and all spectra are presented with respect to the magnetic field range corresponding to a microwave frequency of 9.646000 GHz. Other EPR recording parameters are specified in the figure legend. EPR simulations were carried out as in earlier work (*19*, *41*). All buffers for spectroscopic samples contained 20% 2-propanol to prevent aggregation at high protein concentrations. Purified enzyme stored for up to 2 weeks at 4 °C in Hepes buffer, pH 7.5, containing 20% (v/v) 2-propanol, showed no measurable decrease in activity. Comparison of electronic absorption and EPR spectra with those recorded on more dilute samples in the absence of 2-propanol indicated that 2-propanol had no effect on the electronic structure of the dinuclear metal center (*43*).

RESULTS

Slow-Binding Inhibition of AAP. Peptide thiols of the general structure of **1** (Figure 1) were synthesized and found

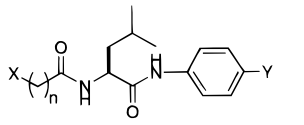

1a	X = SH	n = 1	Y = NO_2
1b	SH	2	NO_2
1c	SH	3	NO_2
1d	SH	3	H
2a	OH	1	NO_2
2b	OH	2	NO_2

FIGURE 1: Structures of AAP inhibitors.

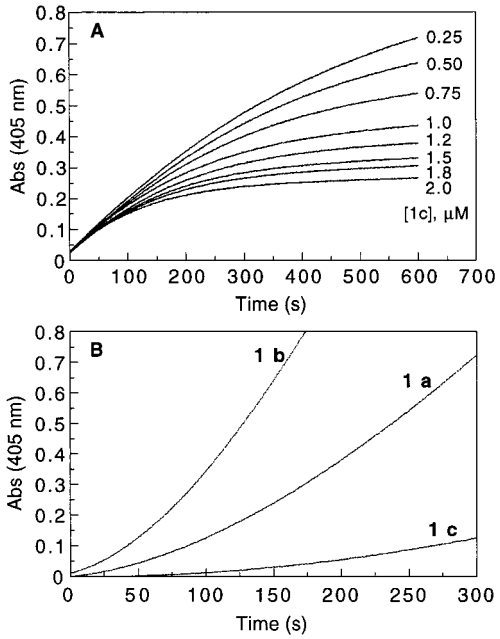

FIGURE 2: Slow-binding inhibition of AAP by peptide thiols **1a**−**c**. (A) Reaction progress for the hydrolysis of Leu-*p*NA (500 μM) in 50 mM Hepes, pH 7.5, 50 mM NaCl, 1 mM TCEP, and 100 μM $ZnSO_4$ and in the presence of the indicated concentrations of **1c**. The reaction was initiated by the addition of 0.01 unit of AAP (0.083 μg) as the last component. (B) Reactivation of AAP that had been treated with inhibitors **1a**−**c**. AAP (320 nM) was incubated with excess **1a**−**c** (10 μM) for 1 h at 0 °C. At time zero, 100 μL of the preincubated AAP/inhibitor complex was used to initiate the hydrolysis of Leu-*p*NA (700 μM for **1a** and 500 μM for **1b** and **1c**) under the same conditions as in panel A. The first-order rate constant k_6 was determined by fitting the data to the following equation: $\text{Abs} = \nu_s[t - 1/k_6(1 - e^{-k_6 t})]$.

to be potent, time-dependent inhibitors of AAP. Upon careful examination, inhibitors **1a**−**d** resulted in biphasic curves when the hydrolysis of leucyl-*p*-nitroanilide by AAP was monitored in a continuous fashion, indicative of slow-binding inhibition (Figure 2) (*40*). The inhibition kinetics can be described by the following equilibria,

$$E + I \overset{K_I}{\rightleftharpoons} E\cdot I \underset{k_6}{\overset{k_5}{\rightleftharpoons}} E\cdot I^*$$

where K_I is the equilibrium inhibition constant for the formation of the initial complex, E·I, and k_5 and k_6 are the forward and reverse rate constants for the slow conversion of the initial E·I complex into a tight complex E·I*, respectively. The overall potency of the slow-binding inhibitors is described by the overall equilibrium constant, $K_I^* = K_I k_6/(k_5 + k_6)$. Table 1 lists the inhibition constants for thiols **1a**−**d** as well as the corresponding alcohols (**2a**,**b**). Thiol inhibitors **1a**−**c** have similar K_I values (200−260 nM) as well as similar forward rate constants, k_5 (3.0−5.4 min^{-1}). However, the overall potency (K_I^*) differs significantly, with **1c** ($K_I^* = 2.5$ nM) being ∼16-fold more potent than **1a** or **1b**. This is primarily due to the difference in their k_6 values (0.066 min^{-1} for **1c** vs ∼0.9 min^{-1} for **1a**,**b**). This suggests that **1a**−**c** bind to AAP with similar rates but the dissociation of **1c** from the enzyme active site is an order of magnitude slower than that of **1a** or **1b**. Inhibitor **1d**, which is structurally similar to **1c** but does not contain the *p*-nitro group, is 25-fold less potent than **1c** ($K_I^* = 63$ nM for **1d**). This is primarily due to the 10-fold increase in the K_I value (1970 nM for **1d** vs 210 nM for **1c**). The corresponding alcohols (**2a**,**b**) are simple competitive inhibitors and are much poorer inhibitors ($K_I = 23$ and 340 μM for **2a** and **2b**, respectively) (Figure 3). These data suggest that the *p*-nitro group is important for the formation of the E·I complex, whereas the free thiol is involved in the formation of both E·I and E·I* complexes, presumably serving as a metal ligand. As a comparison, we also determined the inhibition constant for bestatin, a known slow-binding inhibitor of AAP (46), under the assay conditions used for **1a**−**d**. A K_I^* value of 10 ± 1 nM was obtained, in agreement with the value (18 nM) reported by Wilkes and Prescott (*46*). The extremely slow binding kinetics of bestatin made it difficult to determine the K_I, k_5, and k_6 values (*46*).

Table 1: Kinetic Constants for AAP Inhibition by Peptide Thiols[a]

inhibitor	K_I (nM)	K_I^* (nM)	k_5 (min^{-1})	k_6 (min^{-1})
1a	200 ± 76	40 ± 10	3.0 ± 1.3	0.76 ± 0.07
1b	260 ± 17	57 ± 3	3.5 ± 0.4	0.98 ± 0.16
1c	210 ± 17	2.5 ± 0.3	5.4 ± 1.5	0.066 ± 0.016
1d	1970 ± 170	63 ± 4	1.7 ± 0.3	0.055 ± 0.004
2a	23300 ± 4300			
2b	360000 ± 37000			
bestatin	ND	10 ± 1	ND	ND

[a] Data reported are the mean ± SD for three or more independent experiments. ND, not determined.

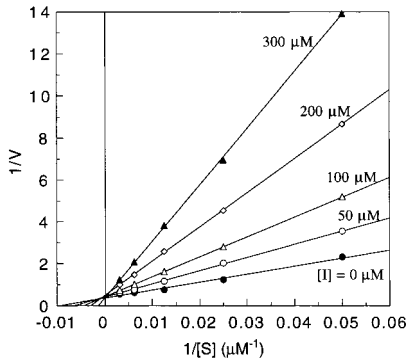

FIGURE 3: Double reciprocal plot velocity ($1/V$) vs substrate concentration 1/[S] in the presence of varying inhibitor **2a** concentrations.

*Electronic Absorption Spectra of **1c** Bound to [CoCo-(AAP)], [CoZn(AAP)], and [CoZn(AAP)]*. Since **1c** is the most potent inhibitor of those tested, its mechanism of inhibition was investigated by electronic absorption spectroscopy using cobalt-substituted AAP. Electronic absorption spectra of [CoZn(AAP)]-**1c** and [ZnCo(AAP)]-**1c** were recorded in the 250−400 nm range. Both Co(II)-substituted AAP enzymes exhibited an absorption band centered at 320 nm in the presence of inhibitor **1c**. Unfortunately, the free ligand (**1c**) also showed a strong absorption ($\epsilon \approx 14\,200$ M^{-1}

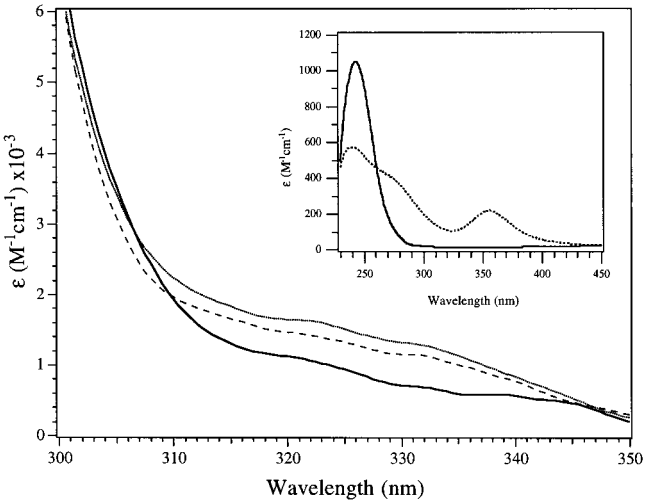

FIGURE 4: Electronic absorption spectra of free AAP and AAP−**1c** complex (after subtraction of the free ligand absorbance). Dotted line, [CoZn(AAP)]-**1c**; dashed lined, [ZnCo(AAP)]-**1c**; solid line, [ZnZn(AAP)] alone. [ZnZn(AAP)], [ZnCo(AAP)], [CoZn(AAP)], and [CoCo(AAP)] all have the same spectrum at 300−350 nm region. Inset: Co(II) + **1c** in 50 mM Hepes (pH 7.5) (dotted line) and Co(II) alone (solid line).

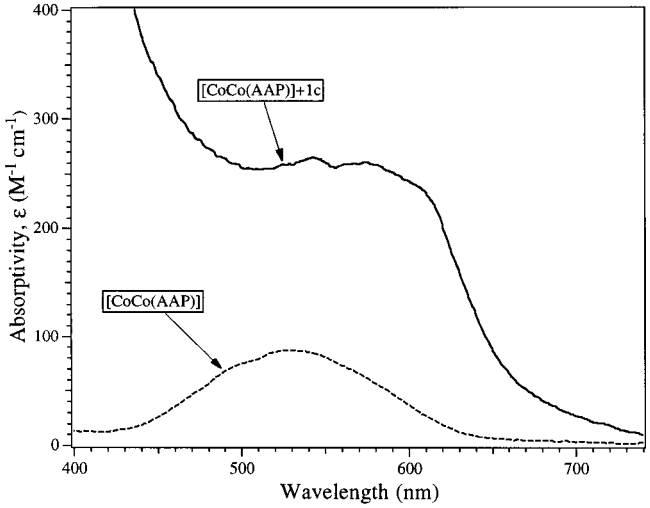

FIGURE 5: Electronic absorption spectrum of [CoCo(AAP)] in the absence (dashed line) and presence (solid line) of 2 equiv of **1c**.

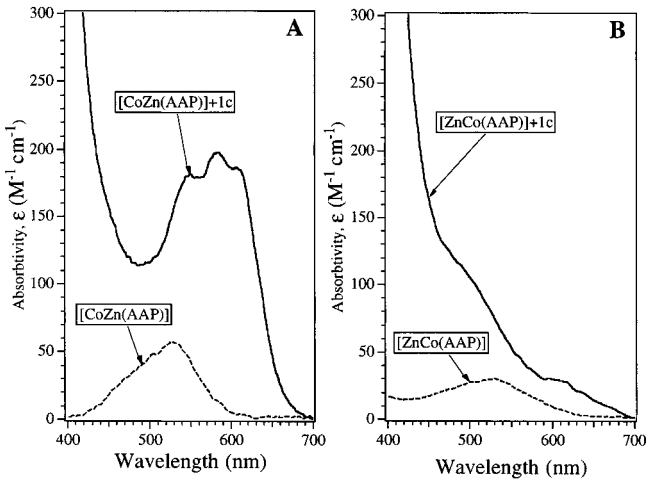

FIGURE 6: (A) Electronic absorption spectrum of [CoZn(AAP)] in the absence (dashed line) and presence (solid line) of 2 equiv of **1c**. (B) Electronic absorption spectrum of [ZnCo(AAP)] in the absence (dashed line) and presence (solid line) of 2 equiv of **1c**.

cm^{-1}) due to the *p*-nitroanilide group. Our attempts to perform the same experiment with **1d**, which lacks the *p*-nitroanilide group, also failed because of the low aqueous solubility of **1d**. Subtraction of the free ligand absorption from that of [CoZn(AAP)]-**1c** or [ZnCo(AAP)]-**1c** shows an increase in absorption at 320 nm over that of free enzyme (Figure 4). This absorption band is very characteristic of an S → Co(II) ligand-to-metal charge-transfer (LMCT) band. As a control, an aqueous sample of Co(II) + **1c** in 50 mM Hepes at pH 7.5 was recorded (Figure 4, inset). These data indicate that, in the absence of enzyme, the S → Co(II) LMCT band is observed at ∼360 nm. Therefore, the absorption band observed at 320 nm, in each of the AAP samples with **1c** present, is likely due to a Co(II)-S−thiolate interaction.

Electronic absorption spectra of [CoCo(AAP)], [CoZn-(AAP)], and [ZnCo(AAP)] were also recorded in the 400−750 nm region and were identical to those previously reported for these species (*17*, *19*, *41*). The absorption due to apo-AAP was subtracted in all cases. The absorption spectrum of [CoCo(AAP)] (Figure 5) shows an absorption maximum of 525 nm and a molar absorptivity (ϵ) of ∼85 M^{-1} cm^{-1}. Addition of **1c** to [CoCo(AAP)] resulted in a marked change in the optical absorption spectrum (Figure 5). There was a clear shift in λ_{max} from 525 to ∼570 nm and an increase in the absorption coefficient from 85 to 270 M^{-1} cm^{-1}. Furthermore, the spectrum of [CoCo(AAP)]-**1c** exhibited fine structure that comprises at least three absorption bands at 548, 583, and 606 nm. Similar spectral changes were also observed when inhibitor **1a** or L-leucinethiol (*44*) was added to [CoCo(AAP)]. The increase in the absorption coefficient and the appearance of fine structure is an indication that the geometry around one or both of the Co(II) ions is significantly altered upon inhibitor binding and demonstrates the direct interaction of **1c** with the dinuclear active site of AAP.

To ascertain the nature of the geometrical change observed for [CoCo(AAP)] upon binding **1c**, electronic absorption spectra of [CoZn(AAP)] and [ZnCo(AAP)] to which **1c** had been added were recorded (Figure 6). The absorption coefficient of [CoCo(AAP)] (85 M^{-1} cm^{-1}) is essentially the sum of the absorption coefficients of [CoZn(AAP)] (58 M^{-1} cm^{-1}; Figure 6A) and [ZnCo(AAP)] (29 M^{-1} cm^{-1}; Figure 6B) and thus indicates that the individual Co(II) ions in [CoZn(AAP)] and [ZnCo(AAP)] must adopt very similar coordination geometries in their respective substituted enzyme forms as they do in the dinuclear center of [CoCo-(AAP)]. The electronic absorption spectrum of [CoZn(AAP)] is consistent with the Co(II) ion in the first metal-binding site adopting a distorted five-coordinate geometry. On the basis of its low molar absorptivity, the Co(II) ion in the second metal-binding site likely adopts a distorted octahedral or pentacoordinate geometry. Upon the addition of **1c** to [CoZn(AAP)], the absorption coefficient nearly quadrupled to 198 M^{-1} cm^{-1} and the λ_{max} exhibited the same red-shift as that observed for [CoCo(AAP)] (i.e., 525 to ∼570 nm) (Figure 6A). The spectrum also exhibited a similar fine structure pattern to that of **1c** bound to [CoCo(AAP)]. On the other hand, the addition of **1c** to [ZnCo(AAP)] decreased λ_{max} from 525 to 510 nm, but the molar absorptivity increased from 30 to 97 M^{-1} cm^{-1} (Figure 6B). These data indicate that the changes observed in the absorption spectrum of

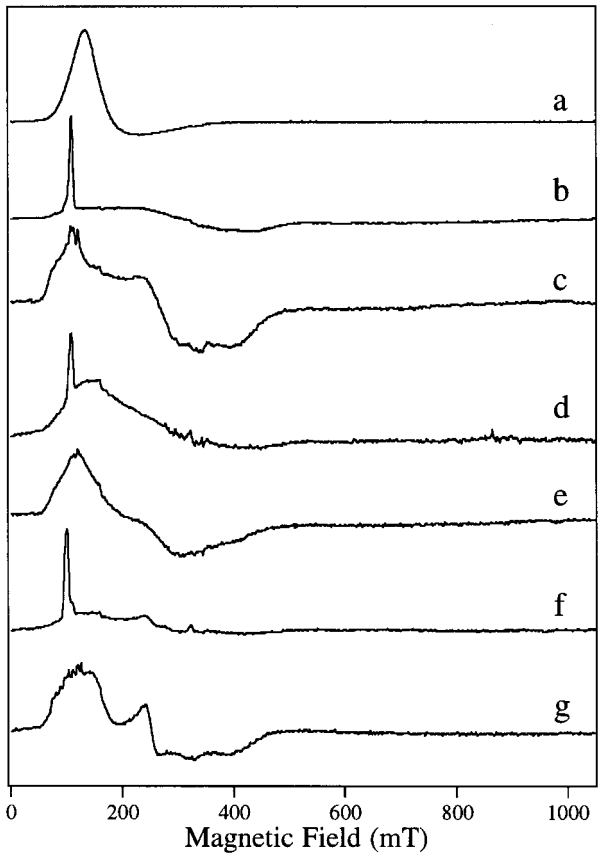

FIGURE 7: EPR Spectra of cobalt-substituted forms of AAP upon addition of inhibitor **1c**. (a) 5 mM $CoCl_2$, 20 mM inhibitor **1c**, recorded at 3.9 K, 50 mW microwave power; (b) [CoCo(AAP)] + **1c**, 4 K, 50 mW; (c) [CoCo(AAP)] + **1c**, 19 K, 0.64 mW; (d) [ZnCo(AAP)] + **1c**, 3.5 K, 50 mW; (e) [ZnCo(AAP)] + **1c**, 18.5 K, 0.8 mW; (f) [CoZn(AAP)] + **1c**, 4 K, 50 mW; (g) [CoZn(AAP)] + **1c**, 19.5 K, 2.5 mW. All samples were buffered with 50 mM Hepes buffer, pH 7.5. All spectra were recorded using 100 kHz modulation frequency, 1.26 mT modulation amplitude, 3.2 mT s^{-1} field sweep rate and 164 ms time constant.

[CoCo(AAP)]-**1c** are primarily due to inhibitor binding to the first metal-binding site; however, **1c** also interacts with the second Co(II) ion.

*EPR Spectroscopy of Co(II)-Substituted AAP Complexes with **1c***. EPR spectra of [Co(AAP)], [CoCo(AAP)], [CoZn(AAP)], and [ZnCo(AAP)] have been recorded previously and are well characterized (*19*, *41*). In the present study, EPR spectra were recorded on the various Co(II)-substituted forms of AAP (i.e., [CoCo(AAP)], [ZnCo(AAP)], and [CoZn(AAP)]) in the presence of **1c** (Figure 7). In each case, two distinct EPR spectra were observed depending on the EPR running conditions. At relatively high temperatures (18−20 K) and modest microwave powers (0.5−2.0 mW), [ZnCo(AAP)] and [CoZn(AAP)] exhibited spectra similar, though not identical to those observed for the uncomplexed forms of the enzyme. For instance, [ZnCo(AAP)] shows a broad, relatively featureless spectrum at 18.5 K, 0.8 mW (Figure 7e) with a barely detectable 7.2 mT hyperfine pattern centered around $g_{eff} \approx 6.9$. The spectrum of the [CoZn(AAP)] complex with **1c** (Figure 7g) at 19.5 K, 2.5 mW, differs from that of the resting signal in that a higher proportion of the hyperfine split signal is observed in the spectrum of the complex. However, the 7.2 mT splitting centered at $g_{eff} \approx 6.92$ and the g_2 feature at $g_{eff} \approx 2.74$ are similar to the corresponding g_{eff} values for the resting enzyme signal of 6.88 and 2.75, respectively. These data establish that in at least some proportion of the enzyme molecules, a weak interaction of **1c** occurs with one of the metal ions, which is sufficient to perturb, but not drastically alter, its resting enzyme EPR signal.

Further information about the nature of the interaction of **1c** with AAP comes from examination of the EPR spectrum of [CoCo(AAP)]-**1c** recorded at 19 K, 0.64 mW microwave power (Figure 7c). Whereas the high-temperature, low-power signals from [ZnCo(AAP)] and [CoZn(AAP)] exhibited some perturbation upon the addition of **1c**, the signal from [CoCo(AAP)] bears no resemblance to that of uncomplexed [CoCo(AAP)] and instead resembles that of [Co(AAP)] (*19*). This implies that a bridging moiety between the cobalt ions, which was proposed to be the μ-OH(H) bridge (*15*, *19*), is lost upon the binding of **1c** with the dinuclear active site. The signal from [CoCo(AAP)]-**1c** is not identical to that of native [Co(AAP)]; in particular, the 7.4 mT splitting pattern is observed at a very high g_{eff} of 7.3. This, in conjunction with the derivative g_2 feature at 2.54 and the g_3 feature at about 1.8, suggests an *E/D* value of ~0.33 compared to 0.28 for [Co(AAP)]. These data imply that both Co(II)-binding sites in AAP are perturbed upon the binding of **1c**.

The high-temperature, low-power EPR data from [CoCo(AAP)]-**1c**, [ZnCo(AAP)]-**1c**, and [CoZn(AAP)]-**1c** indicate that in a given enzyme molecule, **1c** interacts with one of the metal ions in the dinuclear site and that the crystallographically identified μ-OH(H) bridge, which has been shown to mediate electronic interaction of the Co(II) ions (*19*), is broken. The quite subtle changes seen in the EPR spectra compared to those exhibited by isolated Co(II) ions in the uncomplexed forms of the enzyme do not suggest, however, that the interaction which gives rise to the distorted high-temperature, low-power EPR spectra involves direct binding of **1c** via the thiol group. This suggested the possibility that the second metal ion may interact with **1c** through the thiol group yielding a species that does not exhibit an EPR spectrum at high temperatures. We therefore reexamined the EPR samples at lower temperature (3.5−4.0 K) and high microwave power (50 mW) and spectra of [CoCo(AAP)]-**1c**, [ZnCo(AAP)]-**1c**, and [CoZn(AAP)]-**1c** recorded under these conditions are presented as traces b, d, and f in Figure 7. For all three samples, the signals consist of a sharp spike at $g_{eff} = 6.82$ for [CoZn(AAP)] and 6.30 for [CoCo(AAP)] and [ZnCo(AAP)], with a broad underlying absorption. In all cases, the broad absorption resembles the corresponding high-temperature signal. On the basis of these data, it could not be ascertained whether additional features associated with the $g_{eff} = 6.82$ or 6.30 signals were also present along with the incompletely saturated components of the signals characterized at high temperature. Microwave powers of up to 553 mW were employed in an attempt to selectively saturate features not associated with the $g_{eff} = 6.82$ or 6.30 signals. However, severe line-shape distortion at such high powers rendered assignments unreliable.

The observed signals at low temperature could be due to one of two spin states. Where a single feature at $g_{eff} \approx 6.8$ or 6.3 is observed, it is often assumed that the signal corresponds to the g_1 feature of an $M_s = |\pm 3/2\rangle$ transition where $E/D \approx 0$. For an $M_s = |\pm 3/2\rangle$ transition, as $E/D \rightarrow 0$, so g_2 and $g_3 \rightarrow 0$, and the transition probabilities for these resonances also approach zero. Computer simulation (Figure

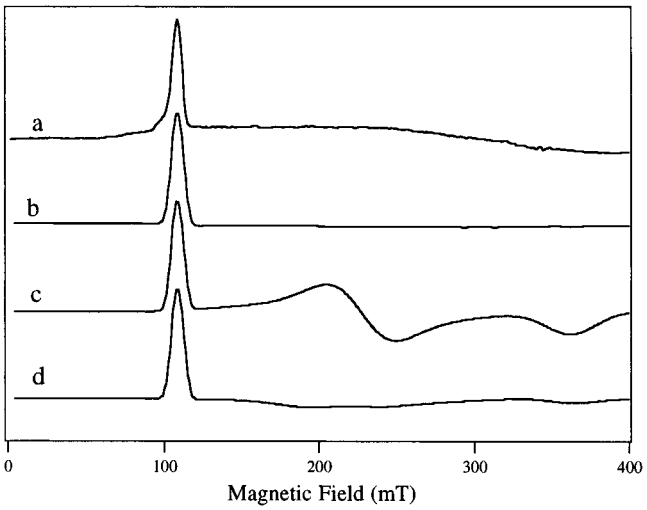

FIGURE 8: Theoretical models for the origin of the $g = \sim 6.8$ or 6.3 feature in the EPR spectra of Co(II)-substituted AAP-**1c** complexes. (a) EPR spectrum of [CoCo(AAP)]-**1c** recorded at 4 K, 50 mW. The sample was buffered with 50 mM Hepes buffer, pH 7.5. The spectrum was recorded using 100 kHz modulation frequency, 1.26 mT modulation amplitude, 3.2 mT s^{-1} field sweep rate and 164 ms time constant; (b) theoretical spectrum generated assuming $M_s = |\pm 3/2\rangle$; $g_{eff(1,2,3)} = 6.30, 0.055, 0.054$; $A^{I=7/2}$ (^{59}Co) = 0, 0, 0 mT. Simulations assuming either isotropic or anisotropic $A(^{59}Co)$ with a range of principal hyperfine coupling constants $A^{I=7/2}_{(1,2,3)}$ (^{59}Co) = ≤ 3, ≤ 3, ≤ 3 mT were essentially indistinguishable; (c) theoretical spectrum generated assuming $M_s = |\pm 1/2\rangle$; $g_{eff(1,2,3)} = 6.30, 3.00, 1.90$; $A^{I=7/2}$ (^{59}Co) = 3.0, 3.0, 3.0 mT; (d), theoretical spectrum generated assuming $M_s = |\pm 1/2\rangle$; $g_{eff(1,2,3)} = 6.30, 3.00, 1.90$; $A^{I=7/2}$ (^{59}Co) = 3.0, 0, 1.0 mT. Line width and *g*-strain parameters were identical for the theoretical spectra b, c, and d.

8b) of a species with $g_{eff(1,2,3)} = 6.31, 0.055, 0.054$, corresponding to $M_s = |\pm 3/2\rangle$, $g_{real} \approx 2.2$ and $E/D \approx 0$, provides a good model for the spectrum of the [CoCo(AAP)]-**1c** complex (Figure 8a) if one assumes the broad absorption from 100 to 550 mT is due solely to incomplete saturation of the other species (Figure 7c). The adoption of an $M_s = |\pm 3/2\rangle$ ground-state implies a reversal in the sign of the zero-field splitting parameter, Δ, which in turn implies a large change in bonding for the Co(II) ion. A second possible origin of this species also exists, however, it is not often considered. Features in the EPR spectrum, particularly the higher field (lower *g*) resonances, due to a high-spin Co(II) ion, in which the paramagnetic electron experiences highly anisotropic coupling to the $I = 7/2$ ^{59}Co nucleus, can appear as a weak and very broad asymmetric signal if the **A** tensor has only a small projection on that particular principal *g* component. A simulation (Figure 8d) for the spectrum of the [CoCo(AAP)]-**1c** complex could thus be obtained assuming $g_{eff(1,2,3)} = 6.31, 3.0, 2.1$, corresponding to $M_s = |\pm 1/2\rangle$, $g_{real} \approx 2.5$ and $E/D \approx 0.25$, including an anisotropic coupling $A_{(1,2,3)} = 3.0, 0.0, 1.0$ mT. This $M_s = |\pm 1/2\rangle$ simulation reproduced the $g = 6.3$ feature equally as well as the $M_s = |\pm 3/2\rangle$ model; however, the presence of weak, broad features in the experimental spectrum of Figure 7b, underlying the residual absorption due to the high-temperature species of Figure 7c, has to be assumed. In contrast, assuming an isotropic **A** tensor yielded a simulation (Figure 8c) in which the prominence of the g_2 and g_3 features preclude this model. The absolute magnitudes of the principal **A** values were not found to be very critical in determining the distribution of intensities of the various features in the simulated spectrum, but their relative values were important. Anisotropy of the hyperfine coupling could arise due to direct binding of a ligand atom such as sulfur onto which extensive electron delocalization could occur.

DISCUSSION

Because of the important physiological roles that aminopeptidases play, our laboratories have been interested in designing highly potent inhibitors for this class of enzymes that can function as both mechanistic probes and potential therapeutic agents. For AAP, several classes of relatively potent inhibitors have previously been investigated, including the natural products amastatin ($K_I = 0.26$ nM) and bestatin ($K_I = 10$ nM), leucine halomethyl ketones ($K_I = 200-700$ nM), 1-butaneboronic acid ($K_I = 9600$ nM), D-leucine hydroxamic acid ($K_I = 2.0$ nM), and L-leucinephosphonic acid ($K_I = 6600$ nM) (*14*, *20*−*28*, *45*−*48*). A common feature of these inhibitors is that they all contain hydrophobic side chains and potential ligands that can coordinate to the metal ions of AAP. Crystallographic studies on the D-iodophenylalanine hydroxamate complex of AAP indicates that the hydroxamate is directly bound to both metal ions in the active site of AAP (*49*). Since thiols are known to be good ligands for Zn(II) cations (*50*), we synthesized *N*-mercaptoacyl-leucyl-*p*-nitroanilide, in anticipation that the N-terminal thiol would ligate to one or both of the Zn(II) ions in the AAP active site. Indeed, peptide thiols **1a**−**c** prove to be excellent inhibitors of AAP, with potencies ($K_I = 2.5$ nM for **1c**) exceeding that of the natural product bestatin and approaching that of amastatin. As compounds **1a**−**c** are readily accessible by synthesis, they provide a new class of potent AAP inhibitors that are also useful for investigating the catalytic mechanisms of aminopeptidases.

Inspection of the observed electronic absorption spectra of [CoCo(AAP)]-**1c**, [CoZn(AAP)]-**1c**, and [ZnCo(AAP)]-**1c** indicates that **1c** interacts with both metal ions. Ligand-field theory predicts that d−d transitions of four coordinate Co(II) complexes give rise to intense absorption ($\epsilon > 300$ M^{-1} cm^{-1}) in the higher wavelength region of 625 ± 50 nm owing to a comparatively smaller ligand-field stabilization energy, while transitions of octahedral Co(II) complexes have very weak absorption ($\epsilon < 30$ M^{-1} cm^{-1}) at lower wavelengths (525 ± 50 nm) (*51*). A five-coordinate Co(II) shows intermediate features: i.e., moderate absorption intensities ($50 < \epsilon < 250$ M^{-1} cm^{-1}) with several maxima between 525 and 625 nm (*51*, *52*). Upon the addition of one equivalent of **1c**, [CoCo(AAP)], [CoZn(AAP)], and [ZnCo(AAP)] give absorption spectra that are very similar to that of the cobalt-substituted angiotensin converting enzyme in the presence of HSAc−Phe-Ala (542, 610, 634 nm, $\epsilon \approx 350, 520, 520$ M^{-1} cm^{-1}) (*53*), AAP in the presence of L-leucinethiol (570 nm, $\epsilon \approx 230$ M^{-1} cm^{-1} with shoulders at 505, 560, and 618 nm) (*44*), and to those of Co(II)-substituted β-lactamase's from *Bacillus cereus* and *Bacteroides fragilis* (530 nm, $\epsilon \approx$ 300 M^{-1} cm^{-1}, with shoulders at 510, 551, 610, 630 nm), which contain a Cys residue as one of the metal ligands (*54*, *55*). All of these enzymes have been proposed to contain five-coordinate Co(II) centers. On the basis of these data, the Co(II) ion in [CoZn(AAP)]-**1c** is likely five-coordinate whereas the Co(II) ion in [ZnCo(AAP)] appears to also reside in a five-coordinate site but a very distorted octahedral

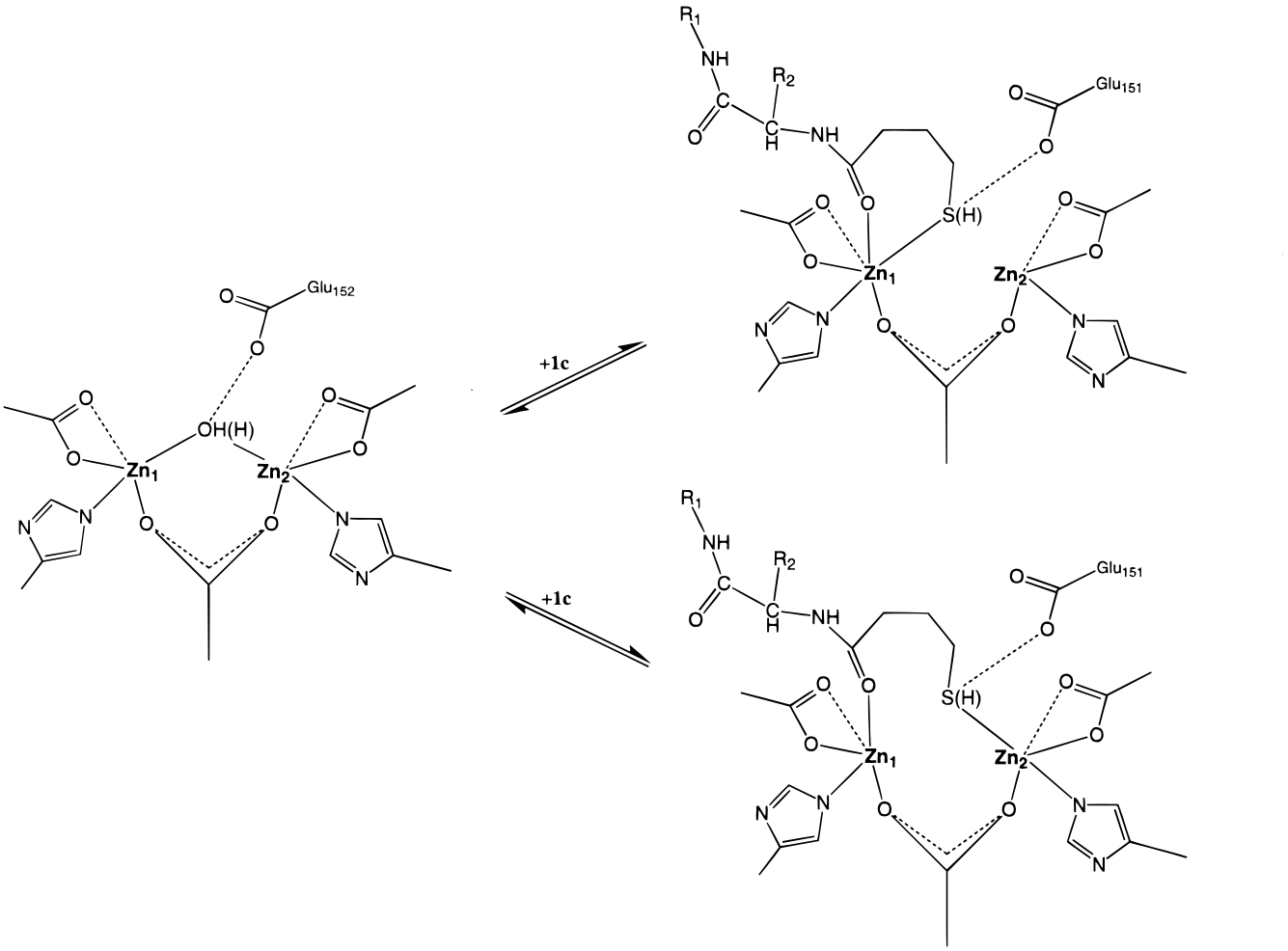

FIGURE 9: Proposed binding scheme of **1c** with the dinuclear active site of AAP.

geometry cannot be discounted. Therefore, it is likely that distortion of each of the Co(II) ions ligand sphere is the cause of a modest change in the electronic structure rather than a change in coordination number. The distortion of both Co(II) ions electronic geometries from complexation by a thiol group is consistent with the observed optical spectral changes.

The EPR spectra observed at $g \approx 6.8$ or 6.3 for each Co(II)-substituted AAP complex of **1c** are striking in that they bear no resemblance to any Co(II) EPR signals observed thus far from Co(II)-substituted AAP and its inhibited complexes (*19*, *24*, *41*). The other striking feature of the observed spectra is that they are all similar to each other. This implies that reaction of **1c** with Co(II) in either of the two sites of the dinuclear center yields electronically similar species. Such a marked change in the EPR signals from those of the Co(II) ions in uncomplexed species of Co(II)-substituted AAP is due to a large perturbation of the electronic structure. Binding of the transition-state analogue inhibitor L-leucinephosphonic acid, which provides an η-1,2-μ-phosphonate bridge between the metal ions and an amine ligand to the second metal ion, has been shown to constrain the geometries around the Co(II) ions and to lead to delocalization of some 30% of the paramagnetic electron density from the amine-liganded Co(II) ion (*24*). Nevertheless, the electronic geometry is not sufficiently perturbed as to result in any drastic change in the g_{eff} and g_{real} values for the hyperfine split species observed in the Co(II)-substituted AAP-L-leucinephosphonic acid complexes compared to those exhibited by uncomplexed Co(II)-substituted enzyme forms. Thus, the low-temperature species observed upon the addition of **1c** to Co(II)-substituted AAP are highly unlikely to arise as a result of an induced change in active-site geometry alone. We, therefore, propose that the novel signals seen at low temperature are the result of direct sulfur ligation of **1c** to both Co(II) ions in the enzyme active site (Figure 9). In support of this proposal, the spectra of a Co(II)-substituted AAP species in the presence of the inhibitors L-leucinethiol and the corresponding alcohol were recently reported (*44*). These data revealed that L-leucinethiol elicits analogous low-temperature signals to **1c**, whereas L-leucinol does not, though leucinol does perturb the EPR signals.

Both the $M_s = |\pm 3/2\rangle$ and $M_s = |\pm 1/2\rangle$ systems described as models for the $g \approx 6.8$ or 6.3 EPR signals could arise as a result of direct sulfur ligation to a Co(II) ion and, thus, analysis of the EPR spectra supports our proposal that **1c** binds to both of the metal ions via the thiol group. At present, there is no definitive way to discriminate between the two models; however, the $M_s = |\pm 1/2\rangle$ model invokes broad features of low intensity in the spectra for which there is no evidence. Therefore, the $M_s = |\pm 3/2\rangle$ model is favored at this time. The observation of a $g_{eff} = 6.8$ or 6.3 EPR signal upon **1c** binding to Co(II)-substituted forms of AAP at low temperature and, of perturbed EPR spectra at high-temperature suggests that **1c** does not discriminate between the two metal ions. Thus, it appears that **1c** can bind to either of the

metal ions through the thiol group. Steric hindrance presumably prevents a second molecule of **1c** from reacting at the active site as well as another functional group on the **1c** molecule to bind to the second metal ion.

Combination of the electronic absorption and EPR data indicates that **1c** perturbs the electronic structure of both metal ions in the dinuclear active site of AAP. Moreover, these data clearly show that in a given population of enzyme, a gross change in electronic structure occurs in both metal ions. The EPR spectra of [CoCo(AAP)] also indicates that the Co−OH(H)−Co bridge is broken upon reaction with **1c**. Because the electronic structure of both metal ions is altered and because the Co−OH(H)-Co bridge is broken, it is tempting to propose that the thiol functionality of **1c** serves to replace the μ-OH(H) bridge and binds to form a Co−S(R)−Co moiety. However, the EPR data is not consistent with such a scenario. While one of the metal ions clearly undergoes a large electronic reorganization, consistent with sulfur ligation, the remaining metal ions display electronic symmetries not unlike those of the analogous, magnetically isolated Co(II) ions in the respective uncomplexed enzyme species. In systems of low symmetry, such as [CoCo(AAP)], [CoZn(AAP)], and [ZnCo(AAP)], significant changes in the electronic properties of the $S = 3/2$ high-spin Co(II) ions are predicted. The observation that one of the Co(II) ions in all of the **1c**-complexed species of AAP studied retained an EPR signal indicative of low electronic symmetry, which was only slightly perturbed from the analogous species in the respective resting enzyme, strongly argues against sulfur ligation to both divalent metal ions via a μ-S(R) bridge. In addition, the spin−spin interaction seen in resting [CoCo(AAP)] is abolished upon the addition of **1c**, and thus, it is unlikely that a single atom bridge is retained or established. Moreover, the lack of any decrease in the ^{59}Co hyperfine splitting in the signals observed at high temperature (19 K) upon addition of **1c** indicates that there is no significant electron delocalization from one of the two active-site metal ions.

Perhaps the most intriguing aspect of the complexation of **1c** by AAP is the slow rate of reaction. The two metal ions in AAP have been shown to be electronically distinct (*19*, *24*, *41*, *56*, *57*), and in the slow reaction with **1c**, one would expect that a preference for one or the other metal ion would be exhibited. Both the EPR and optical data, however, clearly indicate that either, but not both, of the metal ions can bind **1c** via the thiol functionality simultaneously (Figure 9). This implies a lack of exchangeability of the sulfur ligand once bound to the metal, entirely consistent with the very low inhibition constant of **1c**. The slow binding process observed for thiol containing inhibitors may, therefore, involve the nonselective coordination of the thiol moiety to one of the metal ions, followed by the slow deprotonation of the thiol group. Glu151 has been implicated as a general base in the catalytic reaction since it forms a hydrogen bond to the bridging water/(OH^-) group in the resting enzyme; this residue may be responsible for the formation of the thiolate ion (*15*). The reverse process, dissociation of the E·I* complex, would require protonation of the thiolate group. The lack of selectivity of **1c** for a particular metal ion will severely hamper X-ray crystallographic investigations of the precise mode of binding of **1c** to the two metal ions in AAP. Future work will, therefore, require inhibitors that contain functionalities that interact with the substrate-binding pocket in a manner that is sufficiently specific as to uniquely orient the reactive thiol moiety toward one metal ion.

REFERENCES

1. Taylor, A. (1993) *FASEB J. 7*, 290−298.
2. Taylor, A. (1993) *Trends Biochem. Sci. 18*, 167−172.
3. Taylor, A. (1996) in *Molecular Biology Intelligence Unit* (Co., R. G. L., Ed.) pp 1−219, R. G. Landes Co., Austin, TX.
4. Pulido-Cejudo, G., Conway, B., Proulx, P., Brown, R., and Izaguirre, C. A. (1997) *Antivir. Res. 36*, 167−177.
5. Liotta, L. A., Steeg, P. S., and Stetler-Stevenson, W. G. (1991) *Cell 64*, 327−336.
6. Liotta, L. A. (1992) *Sci. Am. 266*, 54−63.
7. Aoyagi, T., Suda, T., Nagai, M., Ogawa, K., Suzuki, J., Takeuchi, T., and Umezawa, H. (1976) *Biochim. Biophys. Acta 452*, 131−143.
8. Fujii, H., Nakajima, M., Aoyagi, T., and Tsuruo, T. (1996) *Biol. Pharm. Bull. 19*, 6−10.
9. Griffith, E. C., Su, Z., Turk, B. E., Chen, S., Chang, Y.-H., Wu, Z., Biemann, K., and Liu, J. O. (1997) *Chem. Biol. 4*, 461−471.
10. Taunton, J. (1997) *Chem. Biochem. 4*, 493−496.
11. Sin, N., Meng, L., Wang, M. Q., Wen, J. J., Bornmann, W. G., and Crews, C. M. (1997) *Proc. Natl. Acad. Sci. U.S.A. 94*, 6099−6103.
12. Lowther, W. T., McMillen, D. A., Orville, A. M., and Matthews, B. W. (1998) *Proc. Natl. Acad. Sci. U.S.A. 95*, 12153−12157.
13. Liu, S., Windom, J., Kemp, C. W., Crews, C. M., and Clardy, J. (1998) *Science 282*, 324−327.
14. Prescott, J. M., and Wilkes, S. H. (1976) *Methods Enzymol. 45B*, 530−543.
15. Chevrier, B., Schalk, C., D'Orchymont, H., Rondeau, J.-M., Moras, D., and Tarnus, C. (1994) *Structure 2*, 283−291.
16. Prescott, J. M., Wagner, F. W., Holmquist, B., and Vallee, B. L. (1983) *Biochem. Biophys. Res. Commun. 114*, 646−652.
17. Prescott, J. M., Wagner, F. W., Holmquist, B., and Vallee, B. L. (1985) *Biochemistry 24*, 5350−5356.
18. Bayliss, M. E., and Prescott, J. M. (1986) *Biochemistry 25*, 8113−8117.
19. Bennett, B., and Holz, R. C. (1997) *J. Am. Chem. Soc. 119*, 1923−1933.
20. Baker, J. O., and Prescott, J. M. (1983) *Biochemistry 22*, 5322−5331.
21. Baker, J. O., Wilkes, S. H., Bayliss, M. E., and Prescott, J. M. (1983) *Biochemistry 22*, 2098−2103.
22. Baker, J. O., and Prescott, J. M. (1985) *Biochem. Biophys. Res. Commun. 130*, 1154−1160.
23. Lejczak, B., Kafarski, P., and Zygmunt, J. (1989) *Biochemistry 28*, 3549−3555.
24. Bennett, B., and Holz, R. C. (1998) *J. Am. Chem. Soc. 120*, 12139−12140.
25. Sträter, N., and Lipscomb, W. N. (1995) *Biochemisty 34*, 9200−9210.
26. Wilkes, S. H., and Prescott, J. M. (1983) *J. Biol. Chem. 258*, 13517−13521.
27. Wilkes, S. H., and Prescott, J. M. (1987) *J. Biol. Chem. 262*, 8621−8625.
28. Chan, W. W.-C., Dennis, P., Demmer, W., and Brand, K. (1982) *J. Biol. Chem. 257*, 7955−7957.
29. Cushman, D. W., Cheung, H. S., Sabo, E. F., and Ondetti, M. A. (1977) *Biochemistry 16*, 5484- 5491.
30. Ondetti, M. A., Condon, M. E., Reid, J., Sabo, E. F., Cheung, H. S., and Cushman, D. W. (1979) *Biochemistry 18*, 1427−1430.
31. Murphy, M. M., Schullek, J. R., Gordon, E. M., and Gallop, M. A. (1995) *J. Am. Chem. Soc. 117*, 7029−7030.
32. Chan, W. W.-C. (1983) *Biochem. Biophys. Res. Commun. 116*, 297−302.

33. Gordon, E. M., Godfrey, J. D., Delaney, N. G., Asaad, M. M., Von Langen, D., and Cushman, D. W. (1988) *J. Med. Chem. 31*, 2199−2211.
34. Beattie, R. E., Elmore, D. T., Williams, C. H., and Guthrie, D. J. S. (1987) *Biochem. J. 245*, 285−288.
35. Corey, E. J., Weinshenker, N. M., Schaaf, T. K., and Huber, W. (1969) *J. Am. Chem. Soc. 91*, 5675−5677.
36. Schalk, C., Remy, J.-M., Chevrier, B., Moras, D., and Tarnus, C. (1992) *Arch. Biochem. Biophys. 294*, 91−97.
37. Chen, G., Edwards, T., D'souza, V. M., and Holz, R. C. (1997) *Biochemistry 36*, 4278−4286.
38. Tuppy, H., Wiesbauer, W., and Wintersberger, E. (1962) *Hoppe-Seyler's Z. Physiol. Chem. 329*, 278−288.
39. Prescott, J. M., Wilkes, S. H., Wagner, F. W., and Wilson, K. J. (1971) *J. Biol. Chem. 246*, 1756−1764.
40. Segel, I. H. (1975) *Enzyme Kinetics: Behavior and analysis of rapid equilibrium and steady-state enzyme systems*, 1st ed., John Wiley & Sons, New York.
41. Bennett, B., and Holz, R. C. (1997) *Biochemistry 36*, 9837−9846.
42. Bennett, B., Berks, B. C., Ferguson, S. J., Thomson, A. J., and Richardson, D. J. (1994) *Eur. J. Biochem. 226*, 789−798.
43. Ustynyuk, L., Bennett, B., Edwards, T., and Holz, R. C. (1999) *Biochemistry 38*, 11433−11439.
44. Bienvenue, D., Bennett, B., and Holz, R. C. (1999) *J. Inorg. Biochem.* (in press).
45. Taylor, A., Peltier, C. Z., Torre, F. J., and Hakamian, N. (1993) *Biochemistry 32*, 784−790.
46. Wilkes, S. H., and Prescott, J. M. (1985) *J. Biol. Chem. 260*, 13154−13162.
47. Kim, H., and Lipscomb, W. N. (1993) *Biochemistry 32*, 8465−8478.
48. Burley, S. K., David, P. R., Sweet, R. M., Taylor, A., and Lipscomb, W. N. (1992) *J. Mol. Biol. 224*, 113−140.
49. Chevrier, B., D'Orchymont, H., Schalk, C., Tarnus, C., and Moras, D. (1996) *Eur. J. Biochem. 237*, 393−398.
50. Cotton, F. A., Wilkinson, G., Murillo, C. A., and Bochmann, M. (1999) *Advanced Inorganic Chermistry*, 6th ed., John Wiley & Sons, New York.
51. Bertini, I., and Luchinat, C. (1984) *Adv. Inorg. Biochem. 6*, 71−111.
52. Horrocks, W., DeW. Jr., I., Holmqust, B., and Thompson, J. S. (1980) *J. Inorg. Chem. 12*, 131−141.
53. Bicknell, R., Holmquist, B., Lee, F. S., Martin, M. T., and Riordan, J. F. (1987) *Biochemistry 26*, 7291−7207.
54. Orellano, E. G., Girardini, J. E., Cricco, J. A., Ceccarelli, E. A., and Vila, A. J. (1998) *Biochemistry 37*, 10173−10180.
55. Crowder, M. W., Wang, Z., Franklin, S. L., Zovinka, E. P., and Benkovic, S. J. (1996) *Biochemistry 35*, 12126−12132.
56. Chen, X.-M., Tong, T.-X., and Mak, T. C. W. (1994) *Inorg. Chem. 33*, 4586−4588.
57. DePaola, C., Bennett, B., Holz, R. C., Ringe, D., and Petsko, G. (1999) *Biochemistry 38*, 9048−9053.

BI991283E